Impact of X-ray Tube Voltage, Field Size and Object Thickness on Scattered Radiation Distribution in Diagnostic Radiology: A Monte Carlo Investigation

P. Ghafarian, *Student Member, IEEE*, M.R. Ay, *Member, IEEE,* H. Ghadiri, S. Sarkar and H. Zaidi, *Senior Member, IEEE*

***Abstract* — The contamination of diagnostic radiology images with scattered photons effectively degrades image quality and decreases low contrast detectability. The magnitude of scattered radiation strongly depends on the object under study and exposure settings. Thorough knowledge of scatter distribution as function of x-ray tube settings and scanning parameters is essential for optimization of system design geometry, selection of imaging protocols and development of optimum anti-scatter grids. The general practice of developing theoretical scatter models involves experimental measurements or deterministic mathematical modeling, whereas most recent publications focus on the use of Monte Carlo simulations. In this study, the general-purpose MCNP4C Monte Carlo computer code was used for calculation of scatter distribution and scatter-to-primary ratio (SPR) as function of tube voltage, field size and object thickness. Scattered radiation was separated from the primary component using the surface source method implemented in the MCNP4C code. The measured spectra published in the Handbook of Computed Tomography X-ray Spectra were used for validation of simulated spectra in the exit window of the x-ray tube and after the phantoms using different materials and thicknesses. Following validation of simulation results, the standard conditions proposed in the IEC 60627 standard were used for scatter distribution characterization. The SPR varied between 0.17 and 13.06 for water phantom thicknesses varying between 3 and 40 cm, whereas it varied between 0.11 and 1.79 for field size varying between 5×5 and 30×30 cm (80 kVp and 20 cm water phantom), and between 2.38 and 2.8 for tube voltages varying between 40 and 150 kVp (30×30 cm field size and 20 cm water phantom), respectively. The results indicate that the MCNP4C code is a useful tool for modelling of scattered radiation in diagnostic radiology provided careful adjustment of the appropriate MCNP cards is carried out by experienced users.**

I. Introduction

The contamination of diagnostic radiology images with scattered photons effectively degrades image quality and decreases low contrast detectability [1]. Therefore considerable research was carried out to develop efficient ways to reduce the amount of scattered radiation reaching the imaging detector in diagnostic radiology imaging. The magnitude of scattered radiation strongly depends on the object under study and exposure settings. Consequently, thorough knowledge of scatter distribution as function of x-ray tube settings and scanning parameters is essential for optimization of system design geometry, selection of imaging protocols and development of optimum anti-scatter grids [2, 3]. The general practice of developing theoretical scatter models involves experimental measurements and mathematical modeling, whereas most recent publications focus on the use of Monte Carlo simulations [2-4]. Monte Carlo calculations have proven to be by far the most successful method for the simulation of the stochastic process of x-ray photons transport in a scattering medium. However, most studies were carried out using in-house or customized developed dedicated Monte Carlo packages [4]. The advantages offered by widely used and extensively tested state-of-the-art general-purpose Monte Carlo codes such as MCNP in terms of versatility, published reports and long term technical support and maintenance are well recognized. In this study the MCNP4C Monte Carlo code was used for calculation of scatter distribution and scatter-to-primary ratio (SPR). The dependence of these parameters on the incident x-ray beam energy (tube voltage), phantom thickness and imaging field size was studied. This information provides a basis for the development of optimum antiscatter grids in diagnostic radiology imaging.

This work was supported by the Research Center for Science and Technology in Medicine, Medical Sciences/University of Tehran and the Swiss National Science Foundation under grant SNSF 3100A0-116547.

Pardis Ghafarain is with the Department of Radiation Medicine, Shahid Beheshti University, Tehran, Iran (email: P.Ghafarian@Mail.sbu.ac.ir).

Mohammad Reza Ay is with the Department of Medical Physics and Biomedical Engineering, School of Medicine, Medical Sciences/University of Tehran, Tehran, Iran and Research Center for Science and Technology in Medicine, Medical Sciences/ University of Tehran, Tehran, Iran (e-mail: mohammadreza_ay@tums.ac.ir).

Hossein Ghadiri is with TPP Co. The authorized distributor of GE Healthcare, Tehran, Iran and Research Center for Science and Technology in Medicine, Medical Sciences/University of Tehran, Tehran, Iran (e-mail: ghadirihossein@tppgems.com)

Saeed Sarkar is with the Department of Medical Physics and Biomedical Engineering, School of Medicine, Medical Sciences/University of Tehran, Tehran, Iran and Research Center for Science and Technology in Medicine, Medical Sciences/ University of Tehran, Tehran, Iran (e-mail: sarkar@tums.ac.ir).

Habib Zaidi is with the Division of Nuclear Medicine, Geneva University Hospital, CH-1211 Geneva, Switzerland (e-mail: habib.zaidi@hcuge.ch).

II. Materials and Methods

A. The MCNP4C Monte Carlo Code

MCNP is a general-purpose, continuous-energy, generalized-geometry, time-dependent, coupled neutron/photon/electron Monte Carlo transport code [5]. For photon transport, the code takes into account photoelectric absorption, with the possibility of K- and L-shell fluorescent emission or Auger electron, coherent and incoherent scattering and pair production. The photoelectric cross sections are based on Storm & Israel [6] whereas the scattering cross sections are taken from ENDF tabulations. The continuous slowing down approximation energy loss model is used for electron transport. To improve the efficiency of electron and photon transport, two cards (PHYS:P and PHYS:E) are implemented in MCNP for biasing some physical parameters such as upper energy limit for electrons and photons (EMAX and EMCPF), production of secondary electrons by photons (IDES), coherent scattering (NOCOH), production of photons by electrons (IPHOT) and production of characteristic x-rays (XNUM).

In the first step, the user should create an input file which contains information about the problem such as geometry specification, description of materials, type of answer or tally and variance reduction techniques to be used. The geometry of MCNP treats an arbitrary three-dimensional configuration in Cartesian coordinate system. The number of cells in this code should be less than 10^5. If this limit is exceeded when using cell geometry, the lattice geometry should be used. The lattice uses a smaller number of cells but adds somewhat to the MCNP execution time. For the purpose of decreasing computation time, MCNP takes advantage of parallel computer architectures. It is supported in multitasking mode on some mainframes and in multiprocessing mode on a cluster of workstations where distributed processing uses the Parallel Virtual Machine (PVM) software.

B. Scattered Radiation Modeling

Scattered radiation was separated from the primary component using the surface source method implemented in the MCNP4C code. In this method, a virtual plane is considered after the scattering medium (water phantom in our experiment) and the direction, energy and history of each photon passing through this plane is recorded. In the next step, the scatter component is calculated by considering only photons which had at least one interaction before hitting this plan toward the detection system. The unscattered component is calculated using the same method by considering only photons which had no interaction before hitting the virtual plane. The pollution of projection data with scattered photons was investigated qualitatively by assessing the distribution of scattered photons as function of phantom size and quantitatively by calculating scatter to primary ratio.

C. Reference Data

The measured spectra published in the Handbook of Computed Tomography X-ray Spectra [7] were used for validation of simulated spectra in the exit window of the x-ray tube and also after the phantoms using different materials and thicknesses [8]. Following validation of simulation results, the standard conditions proposed in the IEC 60627 were used for scatter characterization as function of x-ray tube voltage, field size and phantom thickness [9]. The simulation setup parameters are shown in table 1.

Table1. Summary of Monte Carlo simulation setup (40–120 means from 40 to 120).

Water phantom size (cm)	Field size (cm^2)	Tube voltage (kVp)	Al Inherent filtration (mm)
3–40	30×30	80/120	1.2
20	5×5–30×30	80/120	1.2
20	30×30	40–120	1.2

III. Results

Figure 1 shows the comparison of tungsten x-ray spectra calculated using MCNP4C with measured spectra for the Eimac x-ray tube before and after different phantom thicknesses as benchmark to validate the accuracy of the MCNP4C radiation transport code. This choice was motivated by the fact that experimental measurement of scattered radiation for validation of the code for scatter modeling purposes is very difficult and requires special equipment. It can be seen that simulated results have good agreement with measurements suggesting only slight differences.

Figure 2a shows the magnitude of scattered and primary radiation at 80 and 120 kVp for a water phantom thickness varying between 3 cm and 40 cm. It can be seen that the number of transmitted primary and scattered radiation decreases with increasing the phantom thickness in both tube voltages owing to an increase in the attenuation length in comparison to the mean free path of photons. The peak for the number of scattered photons reflects the trade-off between increasing the probability of Compton scattering and decreasing the transmission probability of scattered photons from the water phantom with increasing the attenuation length.

Figure 2b shows the calculated SPR for different phantom thicknesses at 80 and 120 kVp tube voltages. It can be seen that the SPR increases with increasing phantom thickness as a result of the enhancement of the probability of Compton scattering with increasing the attenuation length. Moreover, the SPR at 120 kVp is higher than at 80 kVp tube voltage. It should be noted that with increasing phantom thickness, the difference between the SPR at 80 kVp and 120 kVp is more

evident owing to an increase of the mean number of interactions and an enhancement of the probability of Compton scattering.

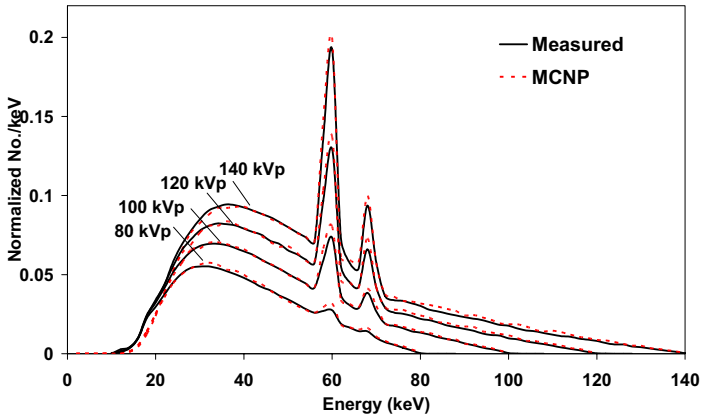

(a)

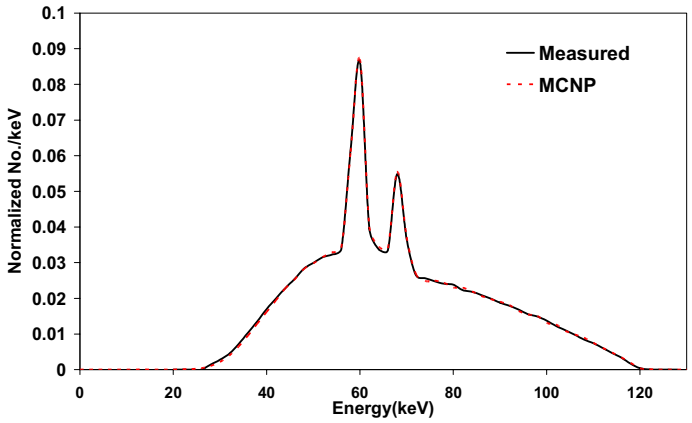

(b)

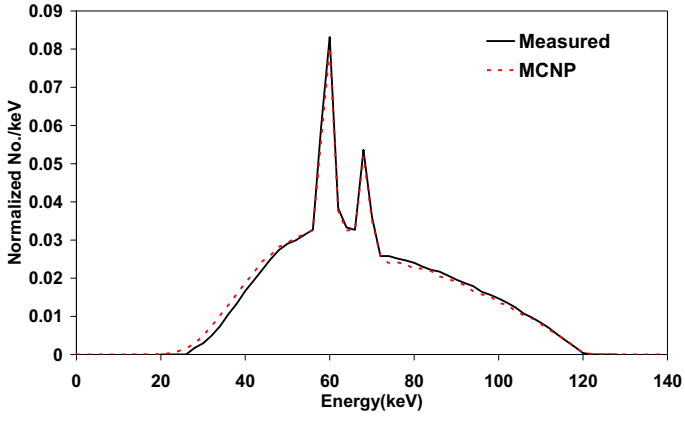

(c)

Figure 1. Comparison of x-ray spectra calculated using MCNP4C with measured spectra at different tube voltages for 12.5° tungsten target, 1.2 mm Aleq inherent filter and FSD of 127 cm; (a) before phantom, (b) after 19.9 cm water and 0.22 cm Lucite phantoms at 120 kVp, and (c) after 25 cm Lucite phantom at 120 kVp.

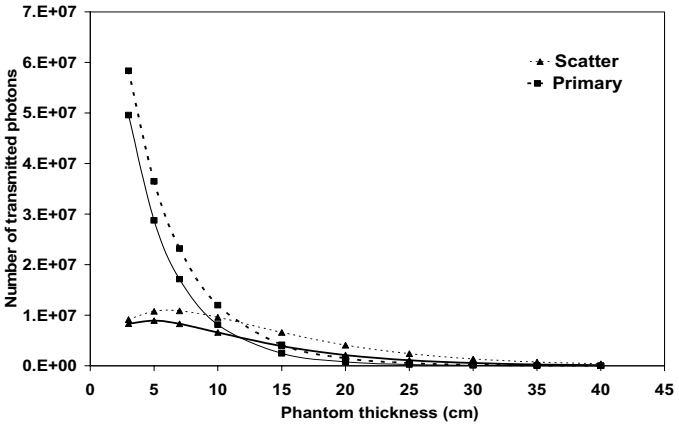

(a)

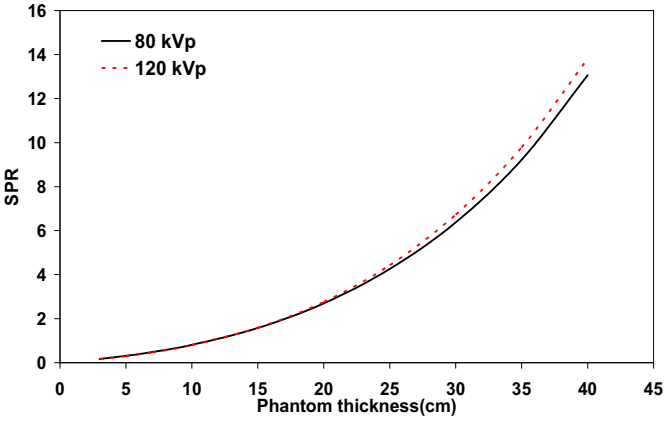

(b)

Figure 2. (a) Magnitude of transmitted primary and scattered radiation at 80 kVp (solid line) and 120 kVp (doted line) tube voltages for different water phantom thicknesses. (b) Plots of SPR vs. phantom thickness at 80 kVp and 120 kVp.

The variation of SPR versus field size and tube voltage is shown in figure 3a. The SPR enhances with increasing field size which is due to an increase in the number of interactions relative to the size of the illuminated object. This effect is more important for smaller field sizes. The magnitude of this effect is directly related to photons energy. Figure 3b shows the variation of SPR as function of tube voltage. The SPR increases rapidly with increasing tube voltage up to 80 kVp, followed by a slow increase reaching a plateau at 120 kVp. Then the curve falls with increasing tube voltage. This behavior could be explained by a rapid increase of the probability of Compton scattering with increasing the tube voltage up to 80 kVp which is offset by an increase of the transmission probability of primary photons with increasing tube voltage after 120 kVp. The SPR varied between 0.17 and 13.06 for water phantom thicknesses varying between 3 and 40 cm, whereas it varied between 0.11 and 1.79 for field size varying between 5×5 and 30×30 cm (80 kVp and 20 cm water phantom), and between 2.38 and 2.8 for tube voltages varying

between 40 and 150 kVp (30×30 cm field size and 20 cm water phantom), respectively.

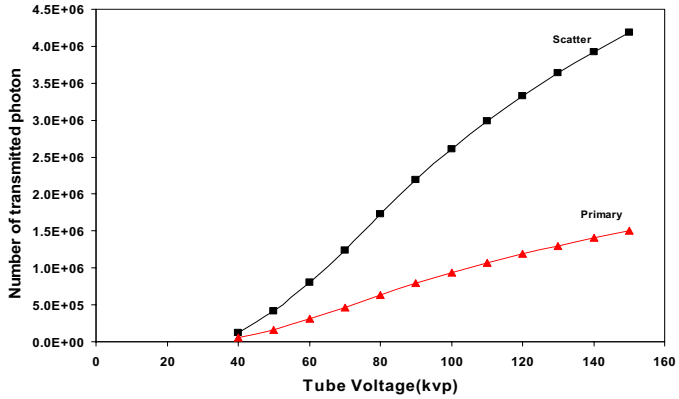

(a)

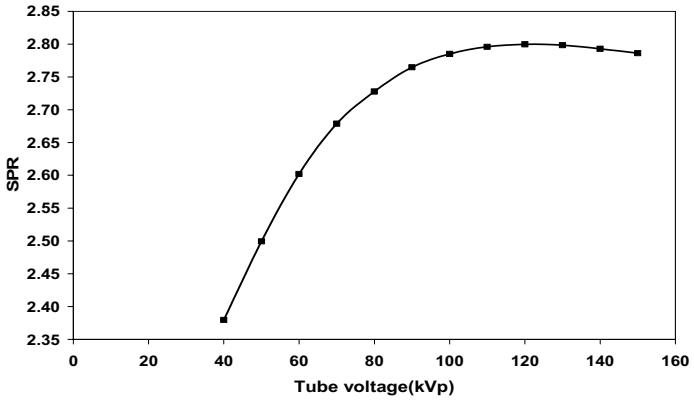

(b)

Figure 3. (a) Magnitude of transmitted primary and scattered radiation at different tube voltages (with 20 cm water phantom), (b) Plots of SPR vs. x-ray tube voltage after 20 cm water phantom.

Figure 4a shows the number of transmitted primary and scattered photons at 80 kVp and 120 kVp as function of field size. Figure 4b also shows the SPR as function of field size for 80 and 120 kVp tube voltages.

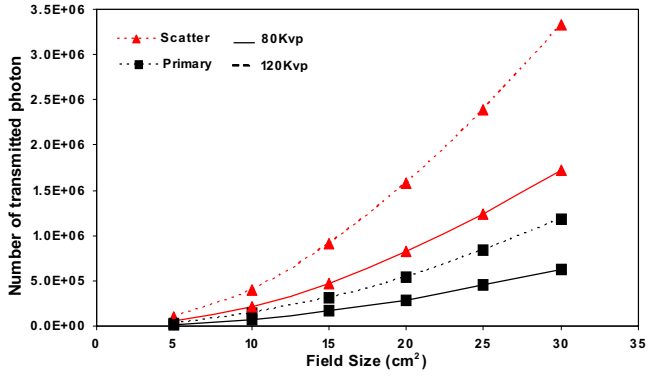

(a)

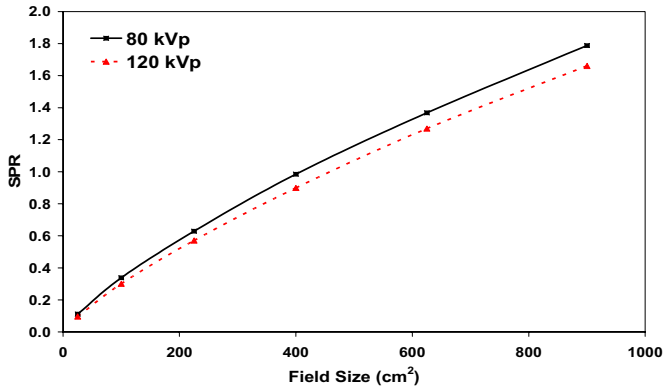

(b)

Figure 4. (a) Magnitude of transmitted primary and scattered radiation vs. field size for 80 and 120 kVp (with 20 cm water phantom), (b) Plots of SPR vs. field size after 20 cm water phantom at 80 kVp and 120 kVp.

Figure 5 shows the influence of additional aluminum filter on number of transmitted photons and SPR at tube voltage of 120 kVp. Figure 5b shows the increasing of SPR with increasing the filter thickness.

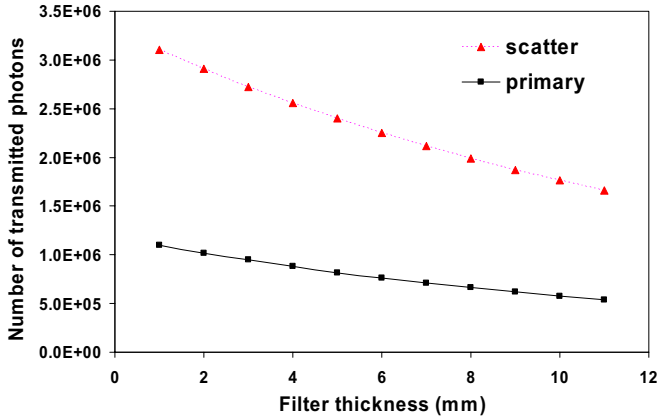

(a)

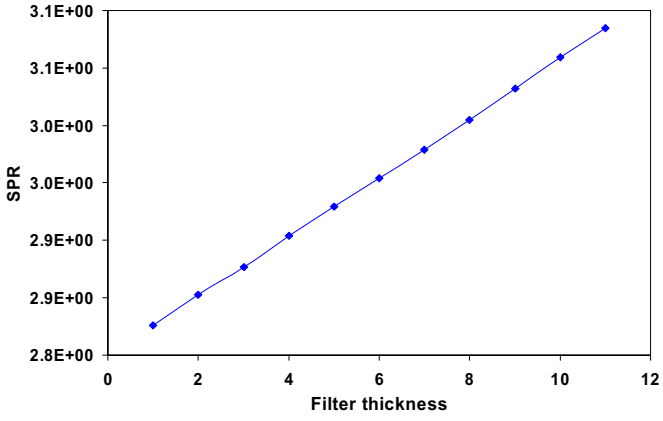

(b)

Figure 5. (a) Magnitude of transmitted primary and scattered radiation for different aluminum filter thicknesses at 120 kVp (with 20 cm water phantom), (b) Plots of SPR vs. aluminum filter thickness after 20 cm water phantom at 120 kVp.

IV. Discussion

In diagnostic radiology, the contrast resolution and low contrast detectability is significantly degraded by scattered radiation. Therefore it is crucial to understand the physical behavior of scattered radiation and the impact of related physical factors such as x-ray tube, object thickness, additional aluminum filter and field of view on the distribution and magnitude of scattered radiation. This information can be used effectively of the optimal design of antiscatter grid in order to remove the contribution of scattered radiation from the projection data in diagnostic radiology imaging. There is a limited number of publications related to experimental measurement of spatial distribution of scattered radiation in tissue equivalent medium owing to the complexity of the experimental setup required for measurement of scatter radiation. It is well accepted that Monte Carlo simulation is one of the most efficient methods for calculation of the distribution and magnitude of scattered radiation. The advantages offered by widely used and extensively tested state-of-the-art general-purpose Monte Carlo codes such as MCNP in terms of versatility, published reports and long term technical support and maintenance are well recognized. In this study, the MCNP4C general purpose Monte Carlo was used for calculation of scattered distribution.

Figure 1 shows the good agreement between simulated and measured results. With increasing the water phantom thickness from 3 cm up to 15 cm at tube voltages of 80 kVp and 120 kVp, the number of transmitted primary photons decreases with a large slope (Fig. 2a). On the other hand, the number of transmitted scattered radiation increases with increasing water thickness until 5 and 7 cm in 80 and 120 kVp, respectively. After these thicknesses, the number of transmitted scattered photons decreases with increasing water thickness. Decreasing the number of transmitted scattered photons is due to absorption into the phantom. Figure 2b shows the increase of SPR with increasing the phantom thickness. This behavior is the result of transmitting more scattered radiation in comparison to transmitted primary radiation. With increasing the phantom thickness, the difference between the SPR at 80 and 120 kVp increases which is due to the increase of the number of scattered radiation in 120 kVp tube voltage. By increasing the tube voltage, the difference between transmitted scattered radiation and primary photons in 20 cm water phantom increases (Fig. 3a), which is due to an increase in the probability of Compton scattering with increasing tube voltage. It has been shown that the SPR increases with increasing tube voltage until 120 kVp and then slightly decreases with increasing tube voltage (Fig. 3b). This is like the result of decreasing the contribution of scattered radiation in high tube voltages. The transmission factor increases with increasing filed size due to the increase in the number of photons in the irradiation area and consequently the increase in the probability of scattering (Fig. 4a). The SPR also increases with increasing the field size at different tube voltages (Fig. 4b) for the same reasons mentioned earlier. The decrease of the number of transmitted scattered and primary photons with increasing the filter thickness is the results of the absorption of radiation in the aluminum filter (Fig. 5a). Increasing the SPR with increasing the filter thickness (Fig. 5b) is due to absorption of photons in the filter and the increase of the probability of Compton scattering.

V. Conclusion

The SPR varied between 0.17 and 13.06 for water phantom thicknesses varying between 3 and 40 cm, whereas it varied between 0.11 and 1.79 for field size varying between 5×5 and 30×30 cm (80 kVp and 20 cm water phantom), and between 2.38 and 2.8 for tube voltages varying between 40 and 150 kVp (30×30 cm field size and 20 cm water phantom), respectively. The results indicate that the MCNP4C code is a useful tool for modelling of scattered radiation in diagnostic radiology provided careful adjustment of the appropriate MCNP cards is carried out by experienced users.

References

[1] H. P. Chan and K. Doi, "Some properties of photon scattering in water phantoms in diagnostic radiology," *Med Phys,* vol. 13, pp. 824-830, 1986.

[2] J. M. Boone, O. V. Makarova, V. N. Zyryanov, C. M. Tang, D. C. Mancini, N. Moldovan, and R. Divan, "Development and Monte Carlo analysis of antiscatter grids for mammography," *Technol Cancer Res Treat,* vol. 1, pp. 441-447, 2002.

[3] P. Ghafarian, A. A. Sharafi, K. Keshvarz, and H. Zaidi, "MCNP4C-based Monte Carlo study of grid performance in diagnostic radiology," *Biomedizinische Technik,* vol. 50, pp. 360-361, 2005.

[4] J. M. Boone, M. H. Buonocore, and V. N. Cooper, "Monte Carlo validation in diagnostic radiological imaging," *Med Phys,* vol. 27, pp. 1294-1304, 2000.

[5] J. F. Briesmeister, "MCNP - A general Monte Carlo N-particle transport code. version 4C," Los Alamos National Laboratory, NM, Los Alamos, NM LA-13709-M, 2000.

[6] E. Storm, "Calculated bremsstrahlung spectra for thick tungsten targets," *Phys Rev,* vol. A5, pp. 2328-2338, 1972.

[7] T. R. Fewell, R. E. Shuping, and K. E. Healy, "Handbook of Computed Tomography x-ray spectra," US Government Printing Office, Washington, D.C. HHS publication (FDA), 81-8162, 1981.

[8] M. R. Ay, M. Shahriari, S. Sarkar, M. Adib, and H. Zaidi, "Monte Carlo simulation of x-ray spectra in diagnostic radiology and mammography using MCNP4C," *Phys Med Biol,* vol. 49, pp. 4897-4917, 2004.

[9] IEC 60627: Diagnostic x-ray imaging equipment – characteristics of general purpose and mammographic anti-scatter grids. International Electrotechnical Commission, Geneva, 2001.